Promoting Effect of CeO_2 on the Catalytic Activity of Ba–Y_2O_3 for Direct Decomposition of NO

Yasuyuki Doi,[1] Masaaki Haneda,*[1] and Masakuni Ozawa[2]

[1]Advanced Ceramics Research Center, Nagoya Institute of Technology, 10-6-29 Asahigaoka, Tajimi, Gifu 507-0071

[2]EcoTopia Science Institute, Nagoya University, Furo-cho, Chikusa-ku, Nagoya, Aichi 464-8603

E-mail: haneda.masaaki@nitech.ac.jp
Received: August 5, 2014; Accepted: September 4, 2014; Web Released: January 15, 2015

The effect of CeO_2 additive on the catalytic performance of Ba–Y_2O_3 prepared by coprecipitaion for the direct decomposition of NO was investigated. Although Ba–Y_2O_3 effectively catalyzed NO decomposition, its activity was clearly increased by addition of CeO_2. The optimum CeO_2 content was 10 mol %. CO_2-TPD measurement revealed that the addition of CeO_2 into Ba–Y_2O_3 caused an increase in the CO_2 desorption peak in the temperature range of 473 and 723 K derived from highly dispersed Ba species. The predominant role of CeO_2 additive was suspected to effectively create the highly dispersed Ba species as catalytically active sites. Kinetic studies of NO decomposition on Ba–CeO_2(10)–Y_2O_3 suggested that coexisting O_2 suppresses the NO decomposition reaction by competitive adsorption. Isotopic transient kinetic analysis suggested a reaction pathway in which the surface NO_x adspecies act as reaction intermediates for the formation of N_2 in NO decomposition over Ba–CeO_2–Y_2O_3. We concluded that CeO_2 additive does not directly participate in the NO decomposition reaction as catalytically active species.

Since nitrogen oxides (NO_x) are harmful to human health and the global environment, the removal of NO_x emitted from combustion facilities is necessary. Use of catalysts is regarded as an effective method for removing NO_x from exhaust gases. For example, three-way catalysts have already been practically applied for the purification of exhaust gas emitted from gasoline-powered vehicles. Selective catalytic reduction of NO_x using urea or ammonia is the leading technology for meeting NO_x emission from diesel exhaust. In these systems, NO_x are efficiently reduced by reacting with reductants such as CO, H_2, ammonia, and hydrocarbons.

On the other hand, direct decomposition of NO ($2NO \rightarrow N_2 + O_2$), which does not require use of reductants and is a thermodynamically favorable reaction, is well known as the most desirable reaction. Therefore, the development of effective catalysts for the direct decomposition of NO is a challenging subject of study for the solution of NO_x problems. Numerous studies have been performed so far to explore catalysts showing activity for the direct decomposition of NO, and have led to the discovery of many active catalysts such as Cu–ZSM[1] and perovskite oxides.[2] However, there is no catalyst that can be used under real conditions in the presence of oxygen, water and carbon dioxide and at high space velocity.

Since oxygen-defect sites are believed to act as active sites for the direct decomposition of NO,[3] the strategy to develop highly active catalysts investigated so far has been to design the catalysts with specific structure promoting oxygen desorption. On the other hand, alkaline earth oxides, which do not include oxygen-deficient sites in the lattice, such as Sr/La_2O_3 and Ba/MgO were reported to effectively catalyze the NO decomposition reaction by Vannice et al.[4] and Lunsford et al.[5,6] One of the authors also reported that the catalytic performance of cobalt oxide can be effectively improved by addition of a small amount of alkali or alkaline earth metals such as K and Ba.[7–9] They proposed a reaction mechanism in which NO_2^- species adsorbed on alkali or alkaline earth metals react with adsorbed NO via the migration of NO_2^- species to the interface between alkali or alkaline earth metals and cobalt oxide.[10]

We have recently investigated the catalytic performance of Ba-doped rare earth oxides prepared by coprecipitation for the direct decomposition of NO, and found that Ba species highly dispersed on rare earth oxides with moderate strength basic sites, such as Dy_2O_3, Sm_2O_3, and Y_2O_3, show relatively high NO decomposition activity.[11,12] The effectiveness of Ba species and Y_2O_3 as catalytically active component and catalyst support, respectively, for the direct decomposition of NO has also been reported by many researchers. For example, Ishihara et al.[13–15] reported Ba containing catalysts such as Ba/BaY_2O_4, Ba/Y_2O_3, and $Ba_3Y_{3.4}Sc_{0.6}O_9$ as highly active catalysts. Tsujimoto et al.[16] studied the additive effect of BaO into C-type cubic Y_2O_3–ZrO_2 solid solution on the NO decomposition performance, and found that Y_2O_3–ZrO_2–BaO catalyst exhibits relatively high NO decomposition activity even in the presence of O_2, H_2O, or CO_2.

Among the catalysts investigated so far, Ba–Y_2O_3 seems to be a highly active catalyst for the direct decomposition of NO. It is of interest that the catalytic performance of Ba–Y_2O_3 continuously increased with the reaction time.[11] This was explained by the creation of highly dispersed Ba sites along with the decomposition of $BaCO_3$ as catalytically inactive species. We also revealed that the formation of $BaCO_3$ is

favorable when Ba species was supported on rare earth oxides with strong basic sites such as La_2O_3.[12] In other words, the selective formation of highly dispersed Ba species can be expected by controlling the surface basicity of Y_2O_3, leading to an increase in the NO decomposition activity. In this study, we have investigated the effect of CeO_2, which possesses weak basicity, on the catalytic activity of Ba–Y_2O_3 for the direct decomposition of NO. The purpose of this work is, accordingly, to specify the importance of controlling the surface basicity of support oxide for the creation of catalytically active Ba species.

Experimental

CeO_2-doped Ba–Y_2O_3 was prepared by coprecipitation using $(NH_4)_2CO_3$ as a precipitation agent, with an aqueous solution of yttrium(III) nitrate, barium(II) nitrate, and cerium(III) nitrate. The precipitate thus obtained was washed with distilled water, followed by drying and calcination at 873 K for 5 h in air. The resulting catalyst powder was finally calcined at 1173 K for 5 h in air. The loading of Ba was fixed at 8 mol %, which was found to be the optimum value,[11] while that of CeO_2 was changed from 1 to 20 mol %. The samples are expressed as Ba–$CeO_2(x)$–Y_2O_3, where x is the loading of CeO_2. The Ba and CeO_2 loadings in the catalysts were estimated by inductively coupled plasma atomic emission spectroscopy (ICP-AES; ICPS-8100, Shimadzu) and documented in Table 1. Cu–ZSM-5 and K/Co_3O_4 with the K/Co atomic ratio of 0.035 as the reference samples were also prepared by the same manner as described elsewhere.[7]

The BET surface area of the samples was measured using a volumetric adsorption apparatus (Micromeritics, TriStar II 3020) by nitrogen adsorption at liquid nitrogen temperature. X-ray diffraction (XRD) patterns were measured using a Rigaku MiniFlex diffractometer with Cu Kα radiation at 30 kV and 15 mA to characterize the crystal structure of Ba–CeO_2–Y_2O_3 samples. Scanning electron microscopy (SEM; JSM-7000F, JEOL) with energy-dispersive X-ray spectrometry (EDS) was used to investigate the distributions of Y, Ba, and Ce in the Ba–CeO_2–Y_2O_3 samples.

Temperature-programmed desorption of CO_2 (CO_2-TPD) was performed using an atmospheric flow system (BELCAT, BEL Japan). Before CO_2-TPD measurement, the sample was pretreated in a flow of O_2 at 1173 K for 2 h, and then cooled down to 323 K in flowing He. CO_2 adsorption was performed by passing a gas mixture of 0.5% CO_2/He through the sample bed at 323 K for 1 h. After the adsorption gas was purged with He until no CO_2 was detected in the effluent, TPD measurement was carried out up to 950 K at a heating rate of 10 K min^{-1} in flowing He at a flow rate of 30 cm^3 min^{-1}. A quadrupole mass spectrometer (M-201QA-TDM, Canon Anelva) was used to analyze the desorbed CO_2.

The direct decomposition of NO was carried out in a fixed-bed continuous flow reactor. The reaction gas composed of 1000 ppm NO with He as the balance gas was fed to a 0.5 g catalyst that had been pretreated in situ in a flow of He at 1173 K for 8 h at a rate of 30 cm^3 min^{-1} ($W/F = 1.0$ g s cm^{-3}) unless otherwise noted. The reaction temperature was decreased from 1173 to 873 K in steps of 50 K, and the steady-state catalytic activity was measured at each temperature. The effluent gas was analyzed by gas chromatography (Shimadzu GC-8A) using a Molecular Sieve 5A column (for analysis of O_2 and N_2) and a Porapak Q column (for analysis of N_2O). A chemiluminescence NO_x analyzer (Shimadzu NOA-7000) was used to check the stability of the catalytic activity.

The reaction rate of N_2 formation was also measured under nearly differential conditions giving NO conversion in the range of 10–30% by varying the catalytic weight from 0.1 to 0.5 g. The concentrations of the reactants were varied in the range of 500–3000 ppm for NO and 0–5% for O_2 to determine the kinetic parameters at 1073 K.

Isotopic transient kinetics analysis was performed by switching the flowing gas from 1000 ppm ^{14}NO to 1000 pppm ^{15}NO diluted in He at 1173 K for a catalyst sample of 0.5 g. The effluent gas from the reactor was continuously monitored by a quadrupole mass spectrometer (PFEFFER OminiStar) for all the isotopic molecules of NO (at $m/e = 30$ and 31), N_2 (at 28, 29, and 30), and N_2O (at 44, 45, and 46).

Table 1. Physicochemical Properties of Ba–CeO_2–Y_2O_3 Samples

Catalyst	Composition /mol %		BET surface area	Lattice constant of Y_2O_3
	Ba	CeO_2	/m^2 g^{-1}	/nm
Ba–Y_2O_3	6.7	0	16.6	1.060
Ba–$CeO_2(1)$–Y_2O_3	6.8	1.0	14.0	1.061
Ba–$CeO_2(5)$–Y_2O_3	6.9	4.7	15.4	1.063
Ba–$CeO_2(10)$–Y_2O_3	7.1	9.6	14.5	1.065
Ba–$CeO_2(20)$–Y_2O_3	7.2	19	16.9	1.067

Results and Discussion

Physicochemical Properties of Ba–CeO_2–Y_2O_3. Table 1 summarizes the BET surface area of Ba–CeO_2–Y_2O_3 with different CeO_2 content. It appears that no significant difference in the BET surface area was obtained irrespective of CeO_2 content. Figure 1 shows XRD patterns of Ba–CeO_2–Y_2O_3 with different CeO_2 content. Distinct XRD peaks indexed to the cubic phase of Y_2O_3 were observed for all the samples. It should be noted that a shift of XRD peaks due to Y_2O_3 to lower angle was observed when CeO_2 content was increased (Figure 1C). As also given in Table 1, the lattice constant of Y_2O_3 calculated for the XRD peak due to Y_2O_3 (100) at $2\theta = 29.0°$ was increased with increasing CeO_2 content, suggesting the formation of a solid solution. Y^{3+} ions are known to be coordinated by 6 oxide anions in Y_2O_3.[17] According to literature,[18] the ionic radii of Y^{3+}, Ce^{3+}, and Ce^{4+} for 6 coordination are 0.090, 0.101, and 0.087 nm, respectively. Taking into account the fact that the lattice constant of Y_2O_3 was increased with CeO_2 content, Ce^{3+} ions are suspected to be incorporated into Y_2O_3 lattice. It is also noteworthy that the XRD peak assignable to $BaCO_3$ gradually decreased with increasing CeO_2 content (Figure 1B), indicating that the dispersion state of Ba species was improved by addition of CeO_2 into Y_2O_3.

In order to obtain further information on the dispersion state of Ba species, elemental mapping at the microstructural level by SEM-EDS was performed for Ba–Y_2O_3 and Ba–$CeO_2(10)$–Y_2O_3. As can be seen in Figure 2A, an aggregation of Ba

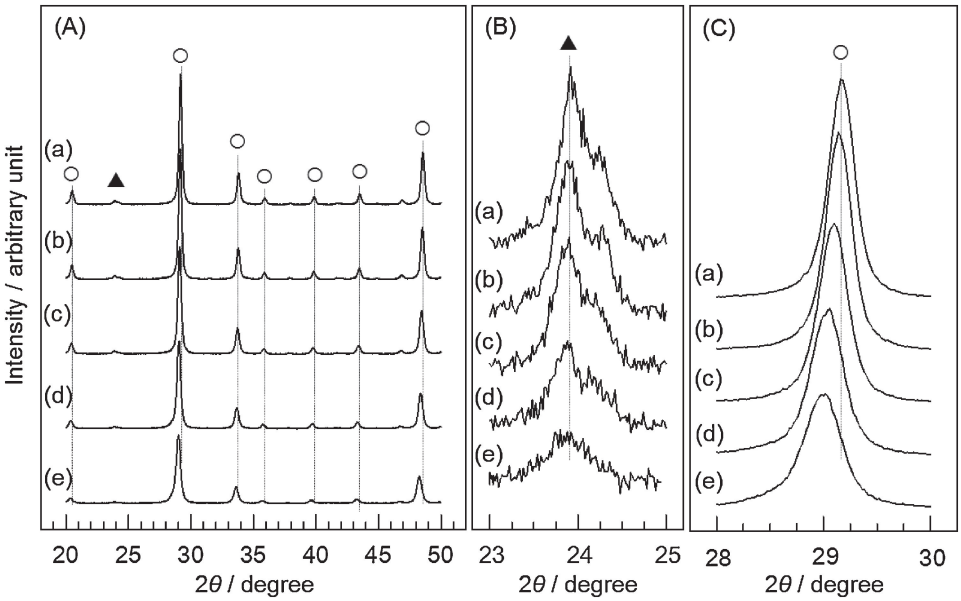

Figure 1. XRD patterns of Ba–CeO_2–Y_2O_3 with various CeO_2 contents. (a) Ba–Y_2O_3, (b) Ba–CeO_2(1)–Y_2O_3, (c) Ba–CeO_2(5)–Y_2O_3, (d) Ba–CeO_2(10)–Y_2O_3, (e) Ba–CeO_2(20)–Y_2O_3. (○) for Y_2O_3, (▲) for $BaCO_3$.

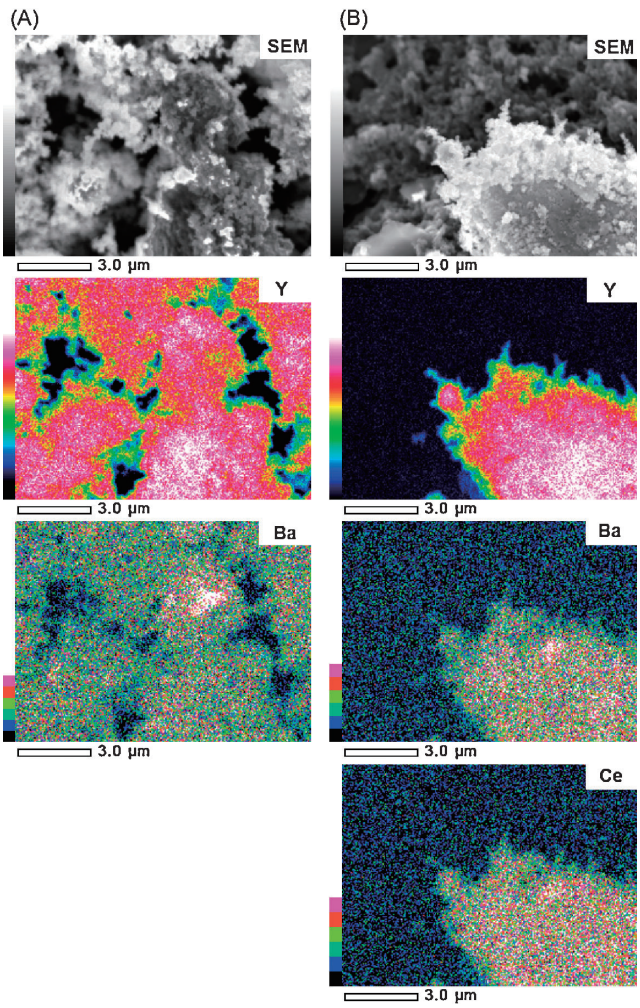

Figure 2. SEM-EDS images of (A) Ba–Y_2O_3 and (B) Ba–CeO_2(10)–Y_2O_3.

species was observed for Ba–Y_2O_3. On the other hand, the formation of relatively well dispersed Ba species was observed for Ba–CeO_2(10)–Y_2O_3 (Figure 2B). In addition, Ba species seems to be present on CeO_2 sites, suggesting the creation of Ba–CeO_2 interaction. In accordance with the results of XRD mentioned above, CeO_2 additive can improve the dispersion state of Ba species.

In our previous study, the formation of $BaCO_3$ was revealed to be favorable when Ba species was supported on rare earth oxides with strong basic sites such as La_2O_3.[12] Therefore, the fact that CeO_2 additive suppressed the formation of $BaCO_3$ may be ascribed to the creation of weak basic sites on the surface of Y_2O_3 by interacting with CeO_2. In order to confirm this assumption, the surface basicity of Y_2O_3 and CeO_2(10)–Y_2O_3 was evaluated by CO_2-TPD measurement. As can be seen in Figure 3a, Y_2O_3 gave three CO_2 desorption peaks at around 391, 512, and 636 K. Although CeO_2(10)–Y_2O_3 showed similar CO_2-TPD profile with Y_2O_3, the presence of CeO_2 caused an increase in the CO_2 desorption at the temperatures below 575 K and a decrease in the CO_2 desorption in the high-temperature region (Figure 3b). In accordance with our assumption, the addition of CeO_2 seems to be lowered the strength of surface basic sites of Y_2O_3, leading to the implementation of the dispersion state of Ba species.

Catalytic Performance of Ba–CeO_2–Y_2O_3 for NO Decomposition. Figure 4 shows the catalytic activity of Ba–CeO_2–Y_2O_3 catalyst with different CeO_2 content for the direct decomposition of NO. A good correlation between N_2 yield and NO conversion was observed (results not shown). O_2 was always formed at a steady state with an O_2/N_2 ratio of approximately unity. The formation of N_2O was hardly observed in the entire temperature range. As can be seen in Figure 4, the NO decomposition activity of Ba–Y_2O_3 was improved by addition of CeO_2. The activity of Ba–CeO_2–Y_2O_3 increased with increasing CeO_2 content, and reached a maxi-

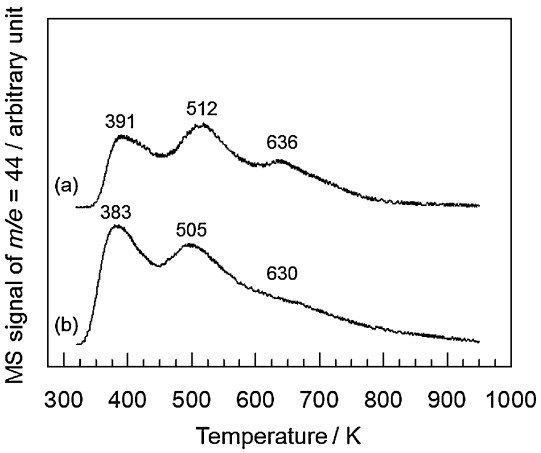

Figure 3. CO_2-TPD profiles of (a) Y_2O_3 and (b) $CeO_2(10)$–Y_2O_3.

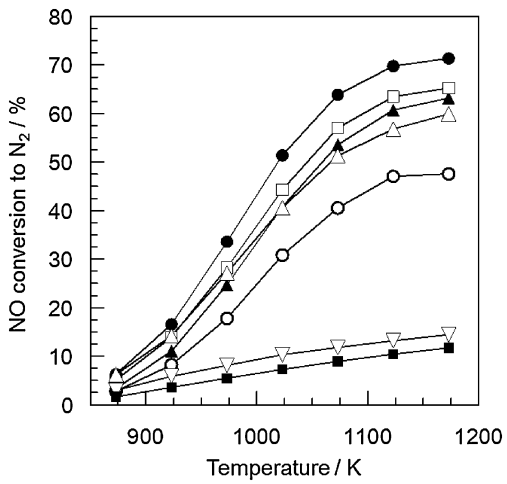

Figure 4. Activity of Ba–CeO_2–Y_2O_3 with various CeO_2 contents for NO decomposition. (▽) Y_2O_3, (■) $CeO_2(10)$–Y_2O_3, (○) Ba–Y_2O_3, (▲) Ba–$CeO_2(1)$–Y_2O_3, (□) Ba–$CeO_2(5)$–Y_2O_3, (●) Ba–$CeO_2(10)$–Y_2O_3, (△) Ba–$CeO_2(20)$–Y_2O_3. Conditions: NO: 1000 ppm, gas flow rate: 30 $cm^3\,min^{-1}$, $W/F = 1.0\,g\,s\,cm^{-3}$.

mum at the CeO_2 content of 10 mol %. Since Y_2O_3 and $CeO_2(10)$–Y_2O_3 showed very low NO decomposition activity, Ba species must be the catalytically active component.

We have recently studied the catalytic performance of Ba-doped rare earth oxide catalysts for NO decomposition, and revealed a good relationship between the N_2 formation rate and the number of Ba species highly dispersed on the surface of rare earth oxide.[12] The number of highly dispersed Ba species was calculated from the amount of CO_2 desorption peak appearing in the temperature range of 573–873 K in the CO_2-TPD profile. In the present study, CO_2-TPD profiles of Ba–CeO_2–Y_2O_3 with different CeO_2 content were measured to evaluate the number of highly dispersed Ba species.

Figure 5 shows the CO_2-TPD profiles of Ba–CeO_2–Y_2O_3 with different CeO_2 content. From the comparison with CO_2-TPD profile of Y_2O_3 given in Figure 3a, the addition of Ba was found to cause a disappearance of two desorption peaks at 512 and 636 K as well as an appearance of new desorption peak at

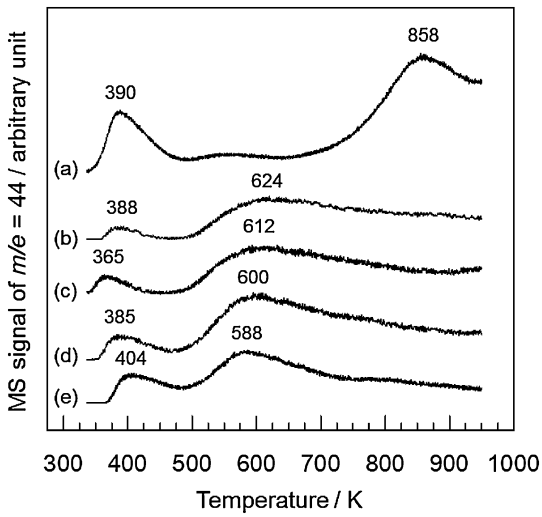

Figure 5. CO_2-TPD profiles of Ba–CeO_2–Y_2O_3 with various CeO_2 contents. (a) Ba–Y_2O_3, (b) Ba–$CeO_2(1)$–Y_2O_3, (c) Ba–$CeO_2(5)$–Y_2O_3, (d) Ba–$CeO_2(10)$–Y_2O_3, (e) Ba–$CeO_2(20)$–Y_2O_3.

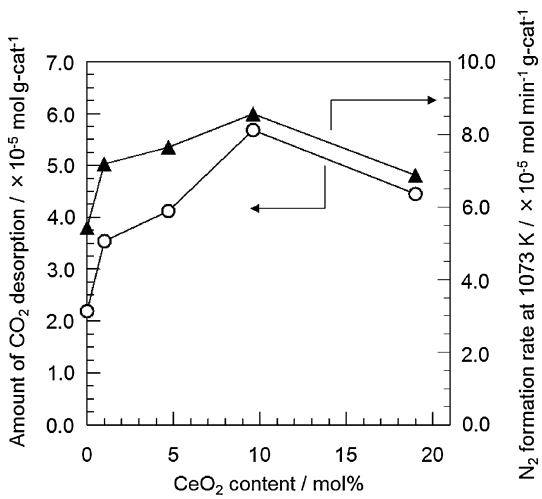

Figure 6. Change in the amount of CO_2 desorption (○) and the rate of N_2 formation at 1073 K (▲) over Ba–CeO_2–Y_2O_3 as a function of CeO_2 content.

858 K, indicating the creation of strong basic sites derived from highly dispersed Ba species. When 1 mol % CeO_2 was added to Ba–Y_2O_3, the CO_2-desorption peak at 858 K was significantly shifted to lower temperature. New CO_2-desorption peak at 624 K was observed. It is of interest that the CO_2 desorption temperature gradually decreased with increasing CeO_2 content. Taking into account the consideration that CO_2 species adsorbed on nanosized Ba sites is easily desorbed at lower temperature, this result clearly indicates that CeO_2 additive can improve the dispersion states of Ba species. This is in agreement with the results of XRD and SEM-EDS analyses.

To gain information on the participation of highly dispersed Ba species as catalytically active sites, the relationship between the amount of desorbed CO_2 in the temperature range of 473–723 K and the rate of N_2 formation at 1073 K was examined. Figure 6 shows the change in the amount of desorbed CO_2, as

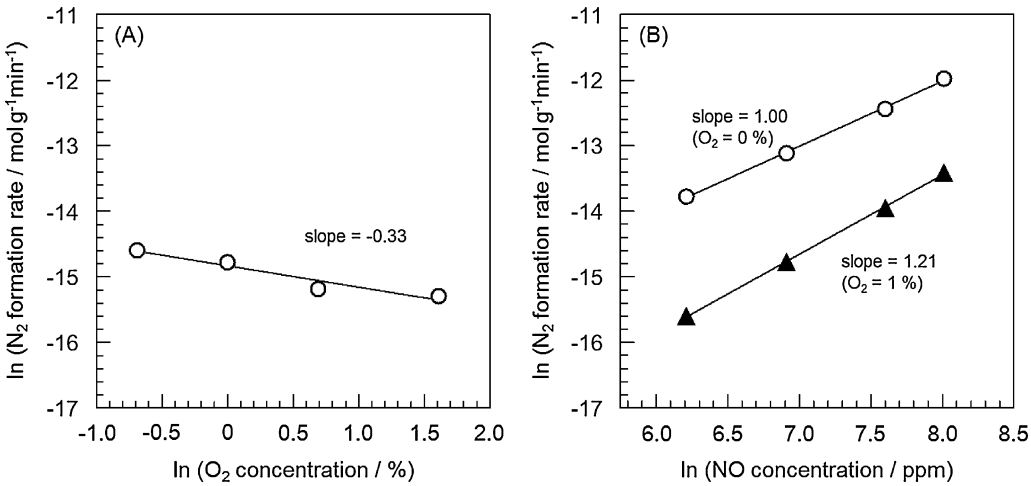

Figure 7. N_2 formation rate over Ba–CeO_2(10)–Y_2O_3 as a function of (A) O_2 (0.5–5%) and (B) NO (500–3000 ppm) in the absence and presence of 1% O_2 at 1073 K. Conditions: NO: 500–3000 ppm, O_2: 0.5–5%, gas flow rate: 30 cm^3 min^{-1}.

well as the N_2 formation rate, as a function of CeO_2 content. It appears that both the amount of desorbed CO_2 and the N_2 formation rate reached the maximum at the CeO_2 content of 10 mol %, indicating that the number of highly dispersed Ba species is responsible for high NO decomposition activity of Ba–CeO_2–Y_2O_3. Since Y_2O_3 and CeO_2(10)–Y_2O_3 showed very low NO decomposition activity (Figure 3), the predominant role of CeO_2 additive is to effectively create the highly dispersed Ba species as catalytically active sites.

Kinetic Studies of NO Decomposition over Ba–CeO_2–Y_2O_3. Since Ba–CeO_2(10)–Y_2O_3 showed the highest NO decomposition activity, as described above, we performed kinetic studies to gain information on the reaction mechanism. First, the effect of O_2 concentration on the activity of Ba–CeO_2(10)–Y_2O_3 was measured. Figure 7A shows ln–ln plots of N_2 formation rate at 1173 K against the concentrations of O_2. Obviously, the N_2 formation rate decreased with increasing O_2 concentration. The reaction order with respect to O_2 was −0.33. In accordance with literature,[3,17,19–21] this result indicates the inhibitor action of O_2 due to competitive adsorption between NO and O_2 onto the active sites. However, the negative effect by coexisting O_2 seems to be not serious in this case, compared with conventional perovskite oxides such as $La_{0.8}Sr_{o.2}CoO_3$,[3] $La_{0.7}Ba_{0.3}Mn_{0.8}In_{0.2}O_3$,[20] and $Ba_{0.8}La_{0.2}Mn_{0.8}Mg_{0.23}$[21] on which the reaction order with respect to O_2 was −0.81, −0.53, and −0.81, respectively.

Figure 7B shows ln–ln plots of N_2 formation rate over Ba–CeO_2(10)–Y_2O_3 at 1173 K as a function of NO concentration in the absence and presence of 0.1% O_2. The N_2 formation rate was found to monotonically increase with an increase in NO concentration. The reaction order with respect to NO was 1.22 in the presence of O_2 and 1.00 in its absence, suggesting that NO decomposition proceeds via similar reaction pathway irrespective of coexisting O_2.

We have so far measured the kinetic parameters of NO decomposition over alkali metal-doped Co_3O_4 catalysts and reported similar kinetic parameters obtained in this study. Namely, the reaction order with respect to O_2 and NO was −0.37 and 1.29 for K/Co_3O_4 catalyst, respectively.[10] From the

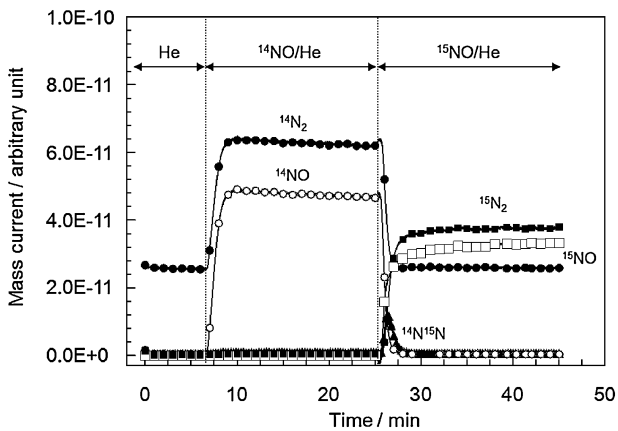

Figure 8. Product responses following the replacement of ^{14}NO/He with ^{15}NO/He in the reaction stream on Ba–CeO_2(10)–Y_2O_3 at 1173 K. (●) $^{14}N_2$, (▲) $^{14}N^{15}N$, (■) $^{15}N_2$, (○) ^{14}NO, (□) ^{15}NO. Conditions: NO: 1000 ppm, gas flow rate: 30 cm^3 min^{-1}, catalyst weight: 0.5 g.

observation of adsorbed NO_x species by in situ FT-IR spectroscopy and isotopic transient kinetic analysis, we proposed a reaction mechanism in which the reaction is initiated by NO adsorption onto alkali metals to form NO_2^- species, which migrates to the interface between the alkali metals and Co_3O_4, and then react with the adsorbed NO species to form N_2. Recently, we have measured FT-IR spectra of NO_x species adsorbed on Ba-doped rare earth oxide under the conditions in flowing NO/He at 873 K, and observed the formation of NO_2^- species irrespective of rare earth oxide.[12] Therefore, it can be expected that NO decomposition reaction over Ba–CeO_2–Y_2O_3 proceeds via similar reaction mechanism proposed for alkali metal-doped Co_3O_4 catalyst.

In order to confirm the possibility mentioned above, isotopic transient kinetic analysis was made on Ba–CeO_2(10)–Y_2O_3. Figure 8 shows the isotopic product responses following the replacement of ^{14}NO/He with ^{15}NO/He in the reaction stream at 1173 K. When ^{14}NO was introduced to the reaction gas, $^{14}N_2$

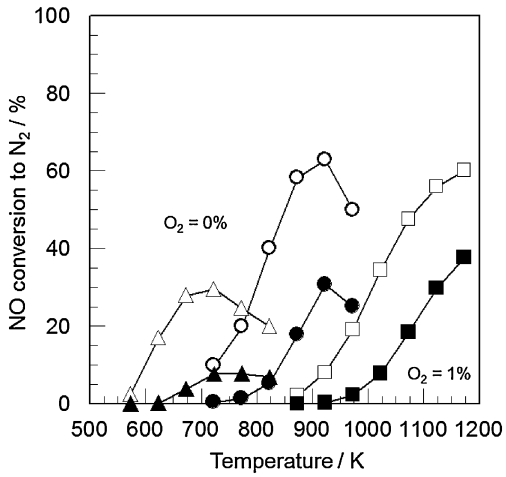

Figure 9. Catalytic activity of Ba–CeO_2(10)–Y_2O_3 (□, ■). Cu–ZSM-5 (△, ▲) and K/Co_3O_4 (K/Co = 0.035) (○, ●) for NO decomposition in the absence and presence of 1% O_2. Conditions: NO: 1000 ppm, O_2: 0 or 1%, gas flow rate: 30 $cm^3\,min^{-1}$, $W/F = 0.5\,g\,s\,cm^{-3}$. Open symbols (□, △, ○) indicate the results obtained in the absence of O_2, and solid symbols (■, ▲, ●) in its presence.

and O_2 (not shown) were detected as products. In accordance with the results obtained under the steady-state conditions, no formation of $^{14}N_2O$ was observed. When the reaction gas was switched from ^{14}NO/He to ^{15}NO/He, a rapid decrease and increase in the formation of $^{14}N_2$ and $^{15}N_2$ were observed, respectively. It should be noted that the evolution of $^{14}N^{15}N$ was simultaneously identified, indicating that the surface NO_x adspecies act as reaction intermediates in the formation of N_2 in NO decomposition. The dynamic behavior of $^{14}N^{15}N$ formation on Ba–CeO_2(10)–Y_2O_3 is in good agreement with that on alkali metal-doped Co_3O_4 and Ba-doped rare earth oxide catalysts reported so far. Therefore, we can conclude that NO decomposition reaction over Ba–CeO_2–Y_2O_3 proceeds via similar reaction mechanism proposed for alkali metal-doped Co_3O_4 and Ba-doped rare earth oxide catalysts. CeO_2 additive does not directly participate in the NO decomposition reaction as catalytically active sites. The predominant role of CeO_2 additive is to effectively create the highly dispersed Ba species as catalytically active sites.

Comparison of NO Decomposition Activity. Since Ba–CeO_2(10)–Y_2O_3 was found to show relatively high NO decomposition activity even in the presence of O_2 from the kinetic parameters (Figure 7), the catalytic activity of Ba–CeO_2(10)–Y_2O_3 was compared with that of Cu–ZSM-5 and K/Co_3O_4 (K/Co = 0.035) as the reference samples.[7,22] The W/F value was slightly changed from 1.0 to 0.5 $g\,s\,cm^{-3}$ by decreasing the sample weight without changing the reaction gas concentration and gas flow rate. Figure 9 shows the catalytic activity of Ba–CeO_2(10)–Y_2O_3, Cu–ZSM-5 and K/Co_3O_4 for NO decomposition in the absence and presence of 1% O_2. It can be seen that the effective temperatures at which high NO decomposition activity was attained changed depending on the catalyst: 623–823 K for Cu–ZSM-5, 823–973 K for K/Co_3O_4 and above 1023 K for Ba–CeO_2(10)–Y_2O_3. Obviously, the addition of O_2 caused a significant decrease in the catalytic activity. The extent of activity depression by O_2 seems to be different depending on the catalyst. The activity depression of Cu–ZSM-5 was the most prominent, while that of Ba–CeO_2–Y_2O_3 was comparable to that of K/Co_3O_4. It is noteworthy that the maximum NO conversion on Ba–CeO_2–Y_2O_3 was higher than those over Cu–ZSM-5 and K/Co_3O_4.

Conclusion

The catalytic activity of Ba–Y_2O_3 for the direct decomposition of NO was effectively improved by addition of CeO_2. The optimum CeO_2 content was found to be 10 mol %. CO_2-TPD measurements revealed that the addition of CeO_2 into Ba–Y_2O_3 caused a significant shift of CO_2 desorption peak at 858 K ascribed to the desorption of CO_2 adsorbed on highly dispersed Ba species to lower temperatures around 588–624 K. Since the relatively good relationship between the amount of desorbed CO_2 in the temperature range of 473–723 K and the rate of N_2 formation at 1073 K was observed, the number of highly dispersed Ba species is responsible for high NO decomposition activity of Ba–CeO_2–Y_2O_3. From the kinetic studies of NO decomposition on Ba–CeO_2(10)–Y_2O_3, the reaction order with respect to O_2 and NO was found to be −0.33 and 1.00–1.22, respectively, suggesting the inhibitor action of O_2. Isotopic product responses following the $^{14}NO \rightarrow {}^{15}NO$ switch revealed the participation of surface NO_x adspecies being reaction intermediates in NO decomposition. The role of CeO_2 additive is not to directly participate in the NO decomposition reaction as catalytically active sites but to effectively create the highly dispersed Ba species as catalytically active sites.

This study was supported by a Grant-in-Aid for Scientific Research (No. 22350068) from the Ministry of Education, Culture, Sports, Science and Technology of Japan.

References

1 M. Iwamoto, H. Furukawa, Y. Mine, F. Uemura, S. Mikuriya, S. Kagawa, *J. Chem. Soc., Chem. Commun.* **1986**, 1272.
2 H. Yasuda, N. Mizuno, M. Misono, *J. Chem. Soc., Chem. Commun.* **1990**, 1094.
3 Y. Teraoka, T. Harada, S. Kagawa, *J. Chem. Soc., Faraday Trans.* **1998**, *94*, 1887.
4 M. A. Vannice, A. B. Walters, X. Zhang, *J. Catal.* **1996**, *159*, 119.
5 S. Xie, G. Mestl, M. P. Rosynek, J. H. Lunsford, *J. Am. Chem. Soc.* **1997**, *119*, 10186.
6 S. Xie, M. P. Rosynek, J. H. Lunsford, *J. Catal.* **1999**, *188*, 24.
7 M. Haneda, Y. Kintaichi, N. Bion, H. Hamada, *Appl. Catal., B* **2003**, *46*, 473.
8 G. Tsuboi, M. Haneda, Y. Nagao, Y. Kintaichi, H. Hamada, *J. Jpn. Pet. Inst.* **2005**, *48*, 53.
9 M. Haneda, G. Tsuboi, Y. Nagao, Y. Kintaichi, H. Hamada, *Catal. Lett.* **2004**, *97*, 145.
10 M. Haneda, Y. Kintaichi, H. Hamada, *Appl. Catal., B* **2005**, *55*, 169.
11 M. Haneda, Y. Doi, M. Ozawa, *Bull. Chem. Soc. Jpn.* **2011**, *84*, 1383.
12 Y. Doi, M. Haneda, M. Ozawa, *J. Mol. Catal. A: Chem.* **2014**, *383–384*, 70.

13 K. Goto, H. Matsumoto, T. Ishihara, *Top. Catal.* **2009**, *52*, 1776.
14 T. Ishihara, K. Goto, *Catal. Today* **2011**, *164*, 484.
15 K. Goto, T. Ishihara, *Appl. Catal., A* **2011**, *409–410*, 66.
16 S. Tsujimoto, X. Wang, T. Masui, N. Imanaka, *Bull. Chem. Soc. Jpn.* **2011**, *84*, 807.
17 N. Imanaka, T. Masui, *Appl. Catal., A* **2012**, *431–432*, 1.
18 R. D. Shannon, *Acta Crystallogr., Sect. A* **1976**, *32*, 751.
19 W.-J. Hong, S. Iwamoto, M. Inoue, *Catal. Lett.* **2010**, *135*, 190.
20 T. Ishihara, M. Ando, K. Sada, K. Takiishi, K. Yamada, H. Nishiguchi, Y. Takita, *J. Catal.* **2003**, *220*, 104.
21 H. Iwakuni, Y. Shinmyo, H. Yano, H. Matsumoto, T. Ishihara, *Appl. Catal., B* **2007**, *74*, 299.
22 M. Iwamoto, H. Hamada, *Catal. Today* **1991**, *10*, 57.

